LAWRENCE
LIVERMORE
NATIONAL
LABORATORY

LLNL-JRNL-446376

PETN coarsening - predictions from accelerated aging data

A. Maiti, R. H. Gee

August 2, 2010

Propellants and Explosives

Disclaimer

This document was prepared as an account of work sponsored by an agency of the United States government. Neither the United States government nor Lawrence Livermore National Security, LLC, nor any of their employees makes any warranty, expressed or implied, or assumes any legal liability or responsibility for the accuracy, completeness, or usefulness of any information, apparatus, product, or process disclosed, or represents that its use would not infringe privately owned rights. Reference herein to any specific commercial product, process, or service by trade name, trademark, manufacturer, or otherwise does not necessarily constitute or imply its endorsement, recommendation, or favoring by the United States government or Lawrence Livermore National Security, LLC. The views and opinions of authors expressed herein do not necessarily state or reflect those of the United States government or Lawrence Livermore National Security, LLC, and shall not be used for advertising or product endorsement purposes.

PETN coarsening – predictions from accelerated aging data

A. Maiti* and R. H. Gee

Lawrence Livermore National Laboratory, Livermore CA 94550

Abstract:

Ensuring good ignition properties over long periods of time necessitates maintaining a good level of porosity in powders of initiator materials and preventing particle coarsening. To simulate porosity changes of such powder materials over long periods of time a common strategy is to perform accelerated aging experiments over shorter time spans at elevated temperatures. In this paper we examine historical accelerated-aging data on powders of Pentaerythritol Tetranitrate (PETN), an important energetic material, and make predictions for long-term aging under ambient conditions. We develop an evaporation-condensation-based model to provide some mechanistic understanding of the coarsening process.

* Corresponding author, E-mail: amaiti@llnl.gov

1. Introduction

Pentaerythritol Tetranitrate (PETN) is an important energetic molecular crystal [1] with applications ranging from the treatment of cardiovascular diseases [2, 3] to an essential high-explosive component for military applications [4]. The ignition characteristics of PETN powder strongly depend on its porosity level as well as its density, with an optimum porosity level needed to be maintained over a period of years to decades [5]. However, experimental evidence indicates that such powder coarsens (i.e. densifies) over time leading to a reduction in porosity. In order to quantify such reduction, accelerated aging experiments at elevated temperatures have been performed [6-10] with the hope that such behavior can be extrapolated to make predictions on long-term aging under ambient conditions. Previously we have attempted to study this problem at the molecular level using a variety of experimental analysis and atomistic and coarse-grained simulations [11-16]. Although such approach yields useful insights, it cannot in a straightforward manner provide a predictive tool for lifetime assessment of powder coarsening and densification.

In this paper we take a more practical approach in which we analyze a set of historical accelerated-aging data and make room temperature extrapolation from such data. Further, we develop a simple model based on basic molecular kinetic processes in an attempt to understand the underlying coarsening mechanisms of PETN.

2. Coarsening data and lifetime prediction

Traditionally the measurement of powder porosity has involved the method of permeametry in which a gas (like air) is allowed to permeate through a powder bed of known dimensions and the flux measured as a function of the pressure differential across the bed. The flux, which is a direct measure of the powder porosity, can be related to an average particle size $\langle d \rangle$ through an equation derived by Gooden and Smith [17], which forms the basis of the widely used method of Fisher sub-sieve size analysis [18]. It is a common convention to express porosity not in terms of $\langle d \rangle$, but rather the equivalent specific surface area of spherical particles of diameter $\langle d \rangle$, given by $6/(\rho \langle d \rangle)$, where ρ is the crystal density of the material

from which the powder was made (i.e. the density of the powder with zero porosity). To avoid any possible confusion with other methods of measuring specific surface area, e.g. BET [19], we refer to the permeametry-measured specific surface area as the Fisher sub-sieve surface area (FSSA) in the rest of the paper.

For a given powder density, one expects higher impact sensitivity (and lower function time [20]) with increasing FSSA, as has been experimentally observed [21, 22]. An increase in function time can adversely affect device performance. Thus it is important to monitor the change in FSSA of an explosive powder as it ages. The purpose of this paper is to examine the historical data on accelerated decrease of FSSA at elevated temperatures and make long-time extrapolation at room temperature.

Fig. 1 displays historical data of FSSA evolution of PETN powder at temperatures varying between 90 and 125 ^{o}C. The data was measured at Pantex [7] using a Fisher sub sieve sizer on a loose powder sample (density close to 50 % of the theoretical maximum value) and an initial FSSA value of approximately 12.5×10^3 cm^2/g. For each temperature the data shows a sharp initial drop for about $\tau_1 \sim 10$ hours followed by a more gradual decrease at longer times. We have not attempted to analyze the detailed time-dependence of the initial sharp drop because of insufficient experimental data points in that regime. Instead we focus on the coarsened value of FSSA at the end of time τ_1, labeled $FSSA_1$ below, as a function of temperature. Fig. 2 plots $FSSA_1$ as a ratio of the initial value $FSSA_0 = 1.25 \times 10^4$ cm^2/g. In order to fit this data we assume that the FSSA does not change at absolute zero temperature, i.e., $FSSA_1/FSSA_0 = 1$ at $T = 0$ K. Including this point in the graph of Fig. 2 leads to the Arrhenius fit:

$$FSSA_1 / FSSA_0 = 1 - A \exp(-\Delta / k_B T) , \qquad (1)$$

where $A \sim 2.7 \times 10^4$, $\Delta \sim 34.6$ kJ/mol is an effective activation barrier for this process, k_B the Boltzmann constant, and T the temperature in K.

As for the more gradual part of Fig. 1 we explored the following two functional forms:

$$FSSA(t) / FSSA_1 = 1 - \alpha \ln(t / \tau_1) \ ; \qquad (2)$$

$$FSSA(t) / FSSA_1 = (t / \tau_1)^{-\alpha} , \qquad (2')$$

where $t \geq \tau_1$ and α is a decay parameter. Within the experimental duration of 200 hours or less (i.e., $t / \tau_1 <$ 20, see Fig. 1), both forms (2) and (2′) yield essentially the same value of the decay parameter α, as plotted in Fig. 3 as a function of temperature T. Just as in Fig. 2, we assume no change in FSSA at $T = 0$ K. However, unlike Fig. 2, the important point in fitting the parameter α (as a function of temperature) is to estimate its value at room temperature. Thus, more than one scheme was necessary to gauge the errors involved in such fits. Fig. 3 displays two different interpolation schemes: (1) the Stineman-interpolation scheme [23], and (2) an Arrhenius formula of the form,

$$\alpha(T) = A_1 \exp(-\Delta_1 / k_B T) , \qquad (3)$$

where $A_1 \sim 2.2 \times 10^3$, and $\Delta_1 \sim 34.5$ kJ/mol. The two schemes yield essentially identical values at elevated temperatures (T more than ~75 ^{o}C). However, at room temperature the predicted values of α are significantly different, ~ 0.007 by the Stineman-interpolation scheme and ~ 0.002 by the Arrhenius scheme. It should also be noted that α displays a significant amount of scatter as a function of T, including non-monotonic behavior at around 100 ^{o}C, which may be attributed to uncertainty in experimental measurements at these temperatures.

Eqs. (1), (2 or 2′), and (3) can be used to predict the evolution of FSSA as a function of time. Fig. 4 plots such evolution for various temperatures, which compares well with Fig. 1, thus verifying the consistency of our fitted parameters.

Next we use these fits to predict long-term aging behavior at room temperature (25 ^{o}C). As pointed out earlier, any PETN powder is typically annealed at an elevated temperature for tens of hours before long-term deployment as an explosive. As a concrete example, let us consider an initial anneal at 75 ^{o}C for a duration $\tau_2 = 100$ hours. From Fig. 4 one can see that the FSSA value following this anneal is $FSSA_2 \sim 10^4$ cm^2/g. In order to predict how this FSSA will evolve at room temperature (25 ^{o}C) over a period of decades, we express eq. (2, 2') in a differential form, which respectively yields:

$$\frac{\partial}{\partial t} FSSA(t) = -\frac{\alpha}{t} FSSA_1 \quad ; \tag{4}$$

$$\frac{\partial}{\partial t} FSSA(t) = -\frac{\alpha}{t} FSSA(t) \, . \tag{4'}$$

Using the boundary condition that FSSA = $FSSA_2$ at $t = \tau_2$, we can solve eqs. (4, 4') to obtain the following evolution equations for FSSA:

$$FSSA(t) = FSSA_2 - \alpha . FSSA_1 . \ln(t / \tau_2) \, ; \tag{5}$$

$$FSSA(t) = FSSA_2 . (t / \tau_2)^{-\alpha} \, , \tag{5'}$$

where $t \geq \tau_2$. Fig. 5 plots FSSA evolution under long-term aging at room temperature using eqs. (5) and (5') with the decay parameter α estimated both from Stineman-interpolation and the Arrhenius expression (eq. (3)). From these estimates the decrease in FSSA at room temperature over a period of 50 years appears to be in the range of 2-6% of the initially annealed value ($FSSA_2$) (see Fig. 5).

3. Analysis

In order to gain some mechanistic insight into the coarsening process underlying the data in Fig. 1, it is necessary to understand all relevant atomic-level mass-transfer processes. There are broadly two classes of such processes, i.e., (i) evaporation-condensation, in which PETN molecules detach from a particle surface, diffuse through the gas phase, and then condense on the surface of a different particle; and (ii) surface diffusion, in which the molecule undergoes long-term diffusion on (solid) particle surfaces without detaching into the gas phase. For PETN, both these processes are likely operational under the temperature conditions of our interest. A full mathematical description of such molecular-level coarsening is a formidable challenge, especially given the uncertainties in particle size and shape distribution, surface roughness, nature of porosity, etc., and might require incorporating complex processes like sintering.

Nevertheless, to make some progress we proceed with a simple working model about the system, which consists of the following assumptions: (1) a collection of detached spherical particles (which can be corrected for realistic shapes by appropriate eccentricity factors); (2) a surface roughness factor that can evolve over time; (3) inter-particle mass transfer occurring solely through the evaporation-condensation mechanism, while the evolution of surface roughness of each particle being controlled through both surface diffusion and evaporation-condensation.

Below we derive the equations that govern the rate of change of particle sizes with time. The most important thermodynamic driving factor for evaporation-condensation-based coarsening is the Gibb's-Thomson/Kelvin effect [24], according to which the equilibrium pressure of a spherical particle of radius r is given by $P(r) = P_\infty \exp(\alpha / r)$, where $\alpha = \frac{2\sigma\upsilon}{k_B T}$, σ being the surface energy density, and υ the volume of a PETN molecule in the solid (i.e. crystal) phase. In the above P_∞ is the equilibrium pressure of bulk PETN, which is known experimentally [11].

Assuming a set of $\{N_j\}$ particles with discrete radii $\{r_j\}$, and a size-independent roughness factor "s" (which can also be interpreted as the "kink density" or "sticking coefficient" and which can be effectively enhanced by the presence of surface features like small particles, undulations, inclusions, protrusions, etc.) the net addition of molecules per unit time into a particle of radius r from the surrounding gas phase is then given by:

$$\varphi(r) = 4\pi r^2 s(P_{eq} - P(r)) / \sqrt{2\pi m k_B T} = 4\pi r^2 s(P_{eq} - P_\infty \exp(\alpha / r)) / \sqrt{2\pi m k_B T} \ . \qquad (6)$$

In eq. (6) above m is the mass of a PETN molecule, and the equilibrium pressure P_{eq} is given by:

$$P_{eq}(t) = P_\infty \frac{\sum_j N_j r_j^2(t) \exp(-\alpha / r_j(t))}{\sum_j N_j r_j^2(t)} \quad , \qquad (7)$$

which follows from the condition of mass conservation, i.e., $\sum_j N_j \varphi(r_j) = 0$. Given that the rate of volume change of a particle is just a product of $\varphi(r)$ and υ, the rate of change of radius is given by:

$$\frac{dr_j(t)}{dt} = sv(P_{eq}(t) - P_\infty \exp(\alpha / r_j(t))) / \sqrt{2\pi m k_B T} \ . \qquad (8)$$

The specific area FSSA at time t is given by:

$$FSSA(t) = \frac{3}{\rho} \frac{\sum_j N_j r_j^2(t)}{\sum_j N_j r_j^3(t)} , \qquad (9)$$

where ρ = 1.78 g/cm^3 is the bulk PETN density. Note that eq. (9) neglects the contribution of surface roughness to the specific surface area, consistent with FSSA measurements.

Eqs. (6) through (9) can be employed to describe the FSSA evolution of a collection of spherical particles. Assuming a specific bimodal distribution as shown in Fig. 6 (top), the time evolution at a specific temperature (90 ^{o}C) is shown in Fig. 6 (bottom) for various constant (i.e. time-independent) values of the parameter s. When we compare the results of Fig. 6 (bottom) with the experimental behavior of Fig. 1 at 90 ^{o}C (shown by the dotted line in Fig. 6) we immediately recognize that the initial steep part corresponds to a larger value of s (perhaps ~ 0.1), while the flat part mandates a small value of s (~ 0.001). In fact, solving eqs. (6) through (9) at different temperatures and comparing with the behavior of Fig. 1 leads to the following picture: initially the particles start out rough. However, within a short time τ_1 (~ 10 hours) the particles smoothen considerably, with the level of smoothing being higher (i.e. lower s) higher the temperature. For longer times the s does not change as significantly. However, the small values of s lead to a more gradual change in FSSA. In this gradual region other mechanisms might come into play, e.g., particle coalescing through neck formation (sintering) etc., which is not taken into account in our model. We would like to note that small values of s (in the *thousandths*) are indeed consistent with the recently observed rate of mass loss from single crystal surfaces using thermo-gravimetric (TGA) measurements [25].

Fig. 7 shows direct experimental evidence in favor of higher levels of smoothing with increasing temperature. In this experiment the sample was first annealed at a lower T (75 ^{o}C) for 75 hours before exposure to an elevated T (100 ^{o}C) for an additional 100 hours. At the point of temperature change the level

of roughness corresponded to the gradual part of 75 ^{o}C, which was still rougher than the level of smoothness that could have been reached if the sample was annealed at 100 ^{o}C from the very beginning. Once the temperature was switched from 75 ^{o}C to 100 ^{o}C, the sample displayed a faster rate of FSSA loss until the level of smoothness reached that corresponding to the gradual part of 100 ^{o}C.

4. Summary and future work

To summarize, we have used historical data of surface area evolution of PETN at elevated temperatures in order to predict long-term aging effects under ambient conditions. To gauge the uncertainty in fitting procedures, we used two different fits, i.e., an Arrhenius-type fit and a Stineman-interpolation scheme, and find that the specific surface area change at room temperature over 50 years should be within 2-6 % of the initially annealed value. The experimental data indicates a steep initial decrease in FSSA followed by a long-term gradual decrease. We find that such behavior can be explained within the evaporation-condensation-driven coarsening by assuming that initially rough particles undergo rapid surface smoothing (mediated by local surface diffusion of molecules), followed by more gradual coarsening of relatively smooth particles. The degree of smoothness achieved is higher for higher temperatures.

Given the uncertainties in sample quality employed in the historical data presented here, similar measurements on fresh PETN powder samples are currently being performed within our group. Initial data seem to indicate similar patterns as Fig. 1, i.e., a sharp initial decrease followed by more gradual long-term coarsening. However, the actual values of FSSA depend strongly on preparation history, process parameters etc. We are also exploring the effect of adding a controlled amount of various impurities. Details will appear in forthcoming publications.

Acknowledgement: The authors would like to sincerely thank Arnie Duncan and Melissa Moore of the Applied Technology division of BWXT Pantex. This work was performed under the auspices of the U.S. Department of Energy by Lawrence Livermore National Laboratory under Contract DE-AC52-07NA27344.

References:

1. J. Trotter, Bond lengths and angles in pentaerythritol tetranitrate, *Acta Crysta* **1963**, *16*, 698.

2. H. I. Russek, The therapeutic role of coronary vasodilators: glyceryl trinitrate, isosorbide dinitrate, and pentaerythritol tetranitrate, *Am. J. Med. Sci.* **1966**, *252*, 9.

3. B. Fink, E. Bassenge, Association Between Vascular Tolerance and Platelet Upregulation: Comparison of Nonintermittent Administration of Pentaerithrityltetranitrate and Glyceryltrinitrate, *J. Cardiovasc. Pharmacol.* **2002**, *40*, 890.

4. R. Meyer, J. Köhler, A. Homburg (eds.), *Explosives*, Wiley-VCH, **2007**.

5. M. F. Foltz, Aging of Pentaerythritol Tetranitrate (PETN), LLNL-TR-415057, **2009**.

6. V. M. Loyola, S. E. Klassen, Materials and Performance Evaluation of Accelerated Aged XTXSOO3, Sandia Report SAND97-2721C, **1998**.

7. A. A. Duncan, Effects of Thermal Conditions and Time on the Morphology of PETN, International High Explosive Aging Workshop, Monterey, CA, **2002**.

8. A. A. Duncan, PETN sublimation and recrystallization, JOWOG 9 meeting, Aldermaston, Reading, UK, June, **2002**.

9. G. Brown, M. Sandstrom, A. Giambra, J. Archuleta, D. Monroe, Understanding Aging in Pentaerythritol Tetranitrate, ESC Review Presentation, LLNL, **2010**.

10. D. C. Monroe, K. E. Laintz, J. F. Kramer, P. D. Peterson, PETN: variation of Physical and Chemical Characteristics Related to Aging, LANLR Report LA-UR-06-2633, **2006**.

11. A. Maiti, R. H. Gee, Modeling growth, surface kinetics, and morphology evolution in PETN, A. Maiti and R. H. Gee, *Prop. Explos* **2009**, *34*, 489.

12. L. Zepeda-Ruiz, A. Maiti, R. Gee, G. Gilmer, and B. Weeks, Size and habit evolution of PETN crystals – a lattice Monte Carlo study, *J. Cryst. Growth* **2006**, *291*, 46.

13. A. Maiti, L. Zepeda-Ruiz, A. Burnham, R. Gee, Vapor pressure and sublimation rate of molecular crystals – role of internal degrees of freedom, *J. Phys. Chem. B* **2007**, *111*, 14290.

14. L. Zepeda-Ruiz, G. H. Gilmer, A. Maiti, R. Gee, A. Burnham, Evaporation of the (110) surface of PETN, *J. Cryst. Growth* **2008**, *310*, 3812.

15. R. Gee, C. Wu, A. Maiti, Mesoscale model of PETN crystals, *Appl. Phys. Lett.* **2006**, *89*, 021919.

16. G. Zhang, B. Weeks, R. Gee, A. Maiti, Fractal Growth in Organic Thin Films: Experiments and Modeling, *Appl. Phys. Lett.* **2009**, *95*, 204101.

17. E. L. Gooden, C. M. Smith, Measuring average diameter of powders — an air permeation apparatus, *Ind. Eng. Chem. Anal. Ed.* **1940**, *12*, 479.

18. A. A. Duncan, Particle Characterization, Pantex Report PX-70-49, **1970**.

19. S. Brunauer, P. H. Emmett, E. Teller, Adsorption of gases in multimolecular layers, *J. Am. Chem. Soc.* **1938**, *60*, 309.

20. For the definition of function time see, P.W. Cooper, Explosives Engineering, *Wiley-VCH,* New York, **1996.**

21. R. H. Dinegar, R. H. Rochster, M. S. Millican, The effect of specific surface on the explosion times of shock initiated PETN, *Am. Chem. Soc. Div. Fuel Chem.* **1963**, *7*, 17.

22. J. A. Waschl, An investigation of PETN sensitivity to small scale flyer plate impact, *J. Energetic Mater.* **1998**, *16*, 279.

23. R. W. Stineman, A Consistently Well Behaved Method of Interpolation, *Creative Computing* **1980**, *6*, 54.

24. B. Mutaftschiev, The Atomic Nature of Crystal Growth, Springer-Verlag, Berlin **2001**.

25. R. Pitchimani, B. L. Weeks, A. K. Burnham, Quantitative Thermodynamic Analysis of Sublimation Rates Using an Atomic Force Microscope, *J. Phys. Chem. B* **2007**, *111*, 9182.

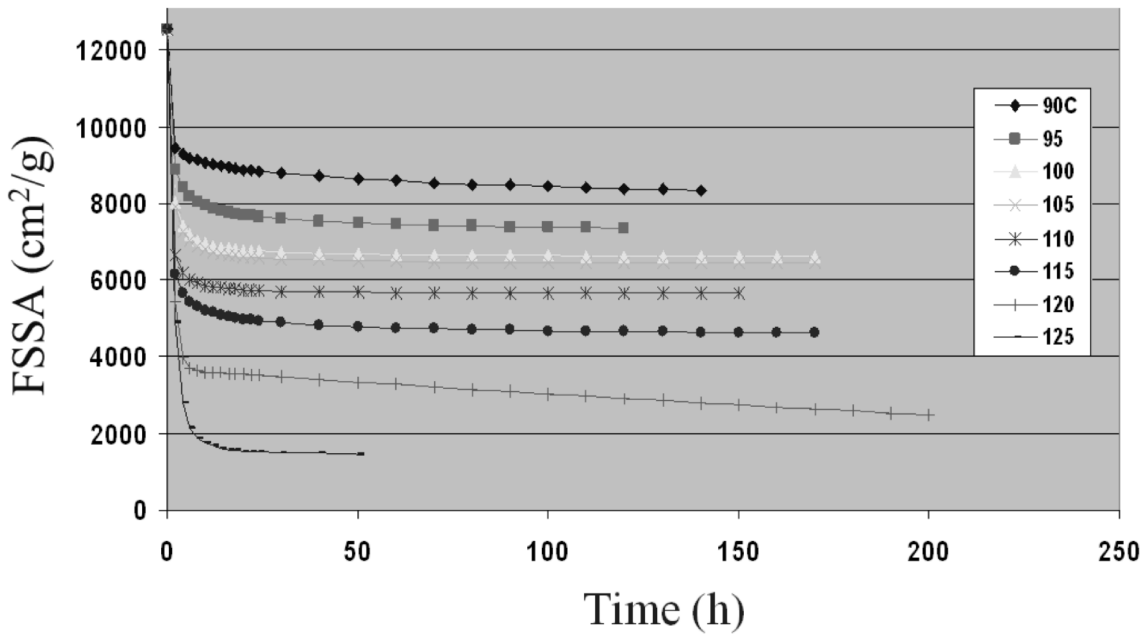

Fig. 1. Time-evolution of the Fisher sub-sieve surface area (FSSA) of a PETN powder at various elevated temperatures. The powder density is ~ 50 % of the theoretical maximum and the initial FSSA is 1.25×10^4 cm^2/g. At each temperature there is a steep initial drop, followed by a more gradual long-term decrease. Despite smoothness of data along each isotherm, there are some inconsistencies due to possible experimental errors, e.g., the 100 ^oC and 105 ^oC data are too close and nearly overlap. Experimental data is from ref. [7].

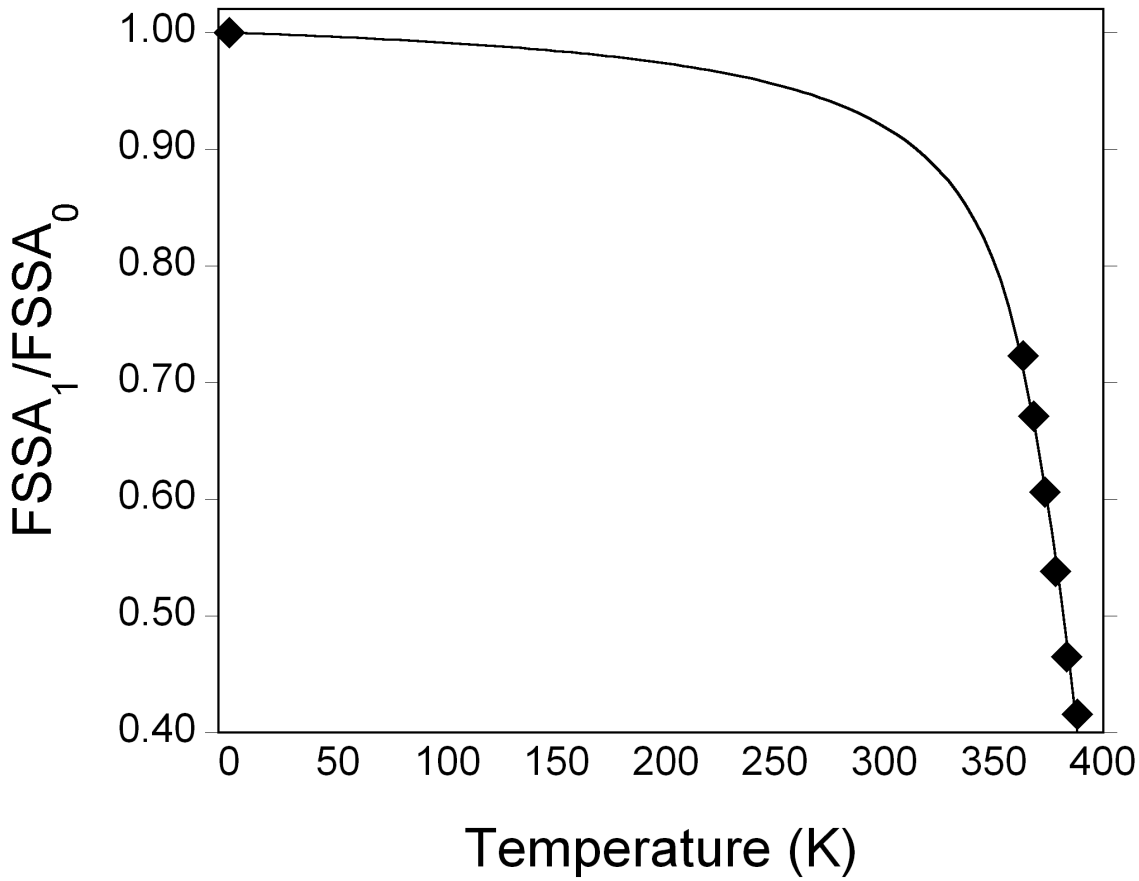

Fig. 2. *Initial steep drop of FSSA as a function of temperature:* Plot of FSSA at time τ_1 = 10 hrs ($FSSA_1$) expressed as a fraction of the initial value ($FSSA_0$). The solid line is an Arrhenius fit of the form: $FSSA_1 / FSSA_0 = 1 - A\exp(-\Delta / k_B T)$, see eq. (1).

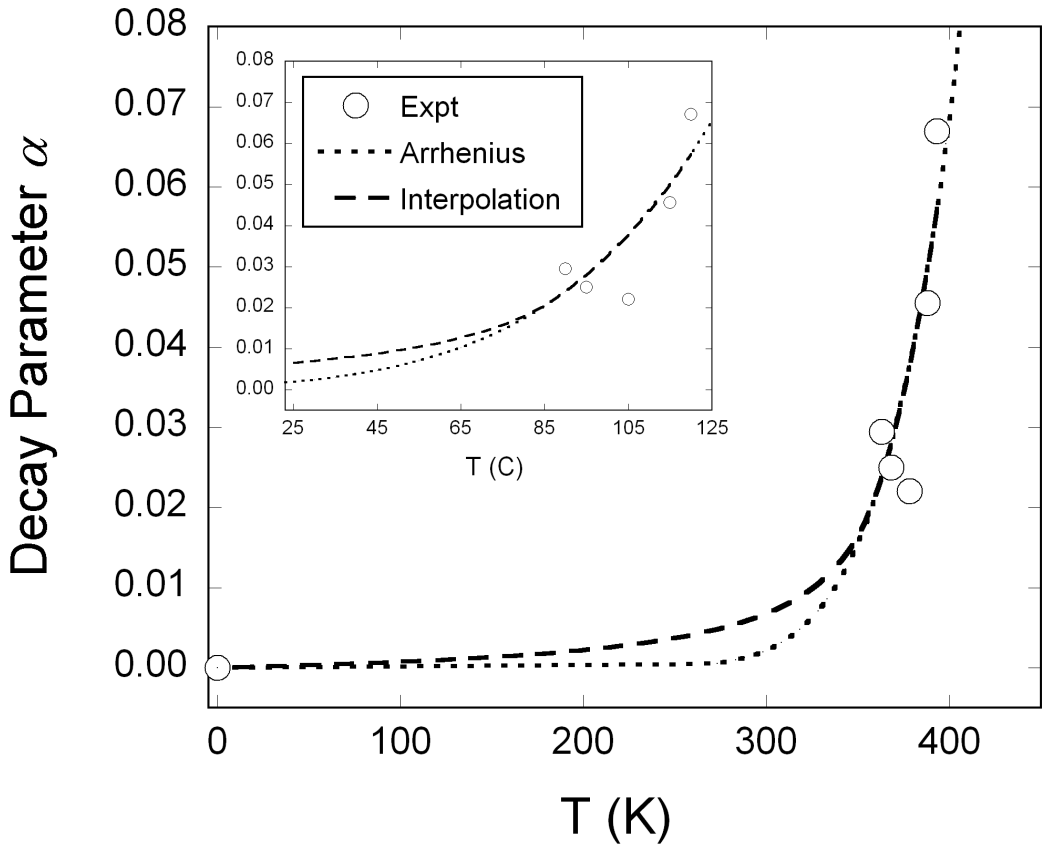

Fig. 3. Plot of the decay parameter α for the slowly evolving part of Fig. 1 (see eq. (2) and (2′)) as a function of temperature T. Experimental points are indicated by circles. The dashed curve is a Stineman-interpolation fit, while the dotted curve is an Arrhenius fit of the form: $\alpha(T) = A_1 \exp(-\Delta_1 / k_B T)$, see eq. (3). (*Inset*) The same plot zoomed in for temperatures between 25 and 125 C.

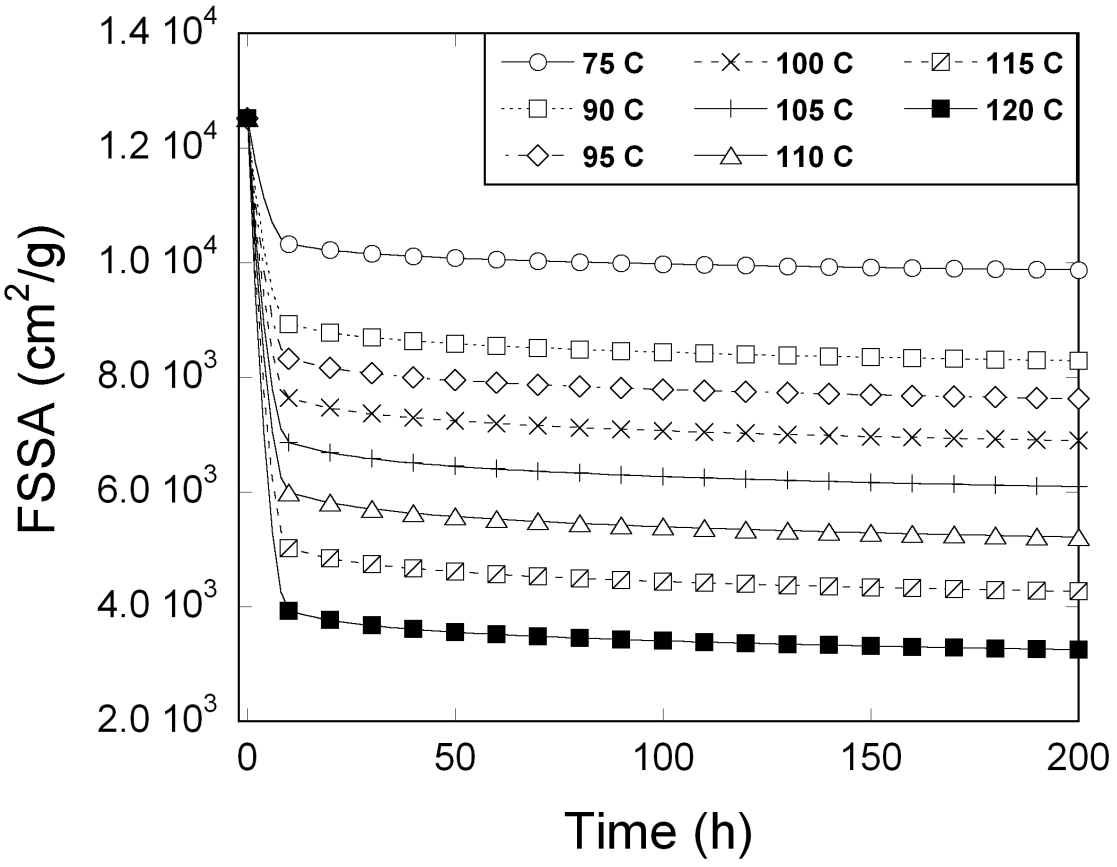

Fig. 4. Evolution of FSSA as a function of time as predicted from eqs. (1), (2), and (3). The results are to be compared with the data of Fig. 1. The various temperatures are indicated in the inset. An extra plot at 75 ^{o}C is included. The evolution curves using eq. (2′) instead of eq. (2) are almost the same, and hence not shown separately.

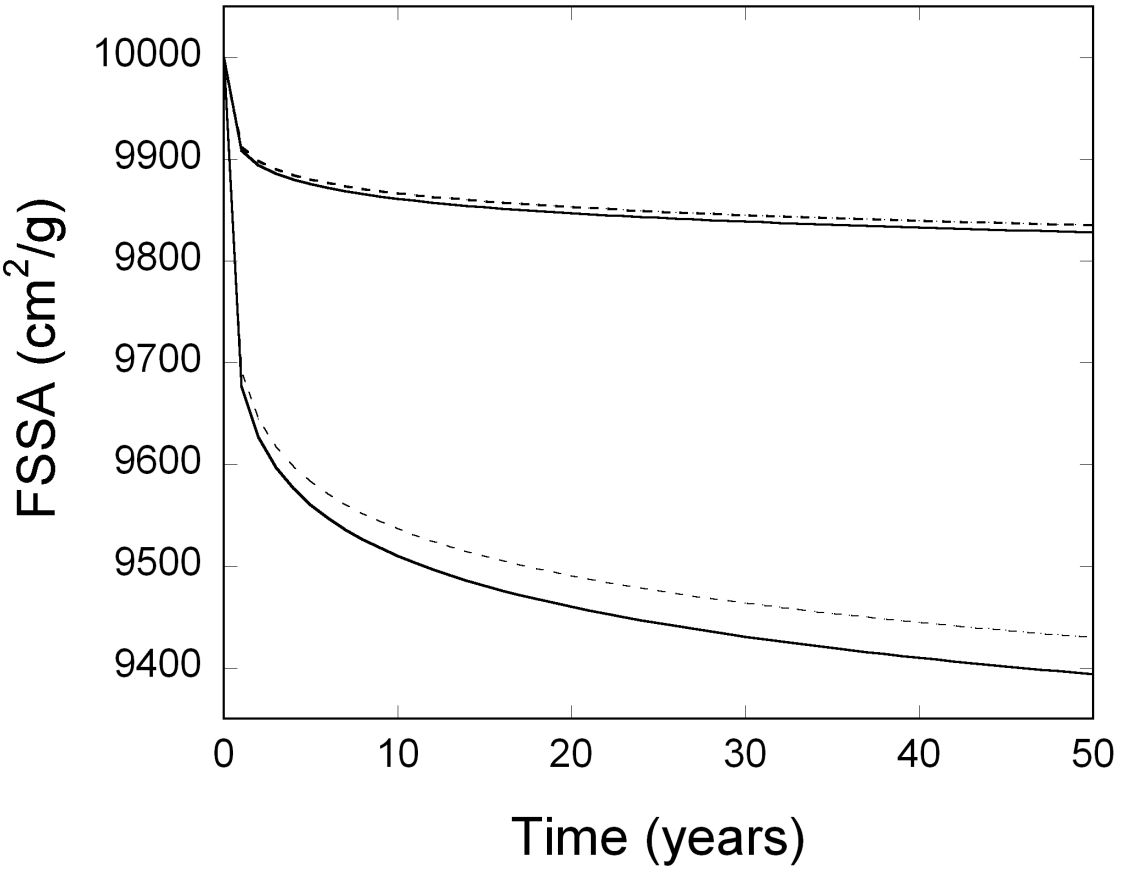

Fig. 5. Prediction of FSSA evolution under long-term aging at room temperature: solid curves are obtained using eq. (5), while dashed curves are obtained with eq. (5'). Upper (lower) set of curves are obtained using values of α at room temperature estimated by the Arrhenius (interpolation) schemes respectively.

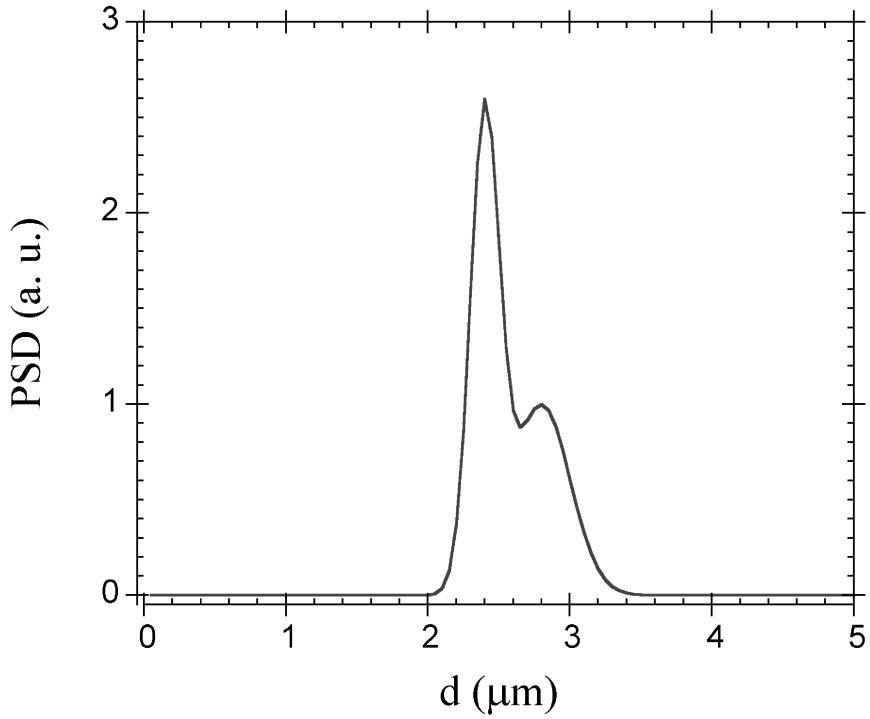

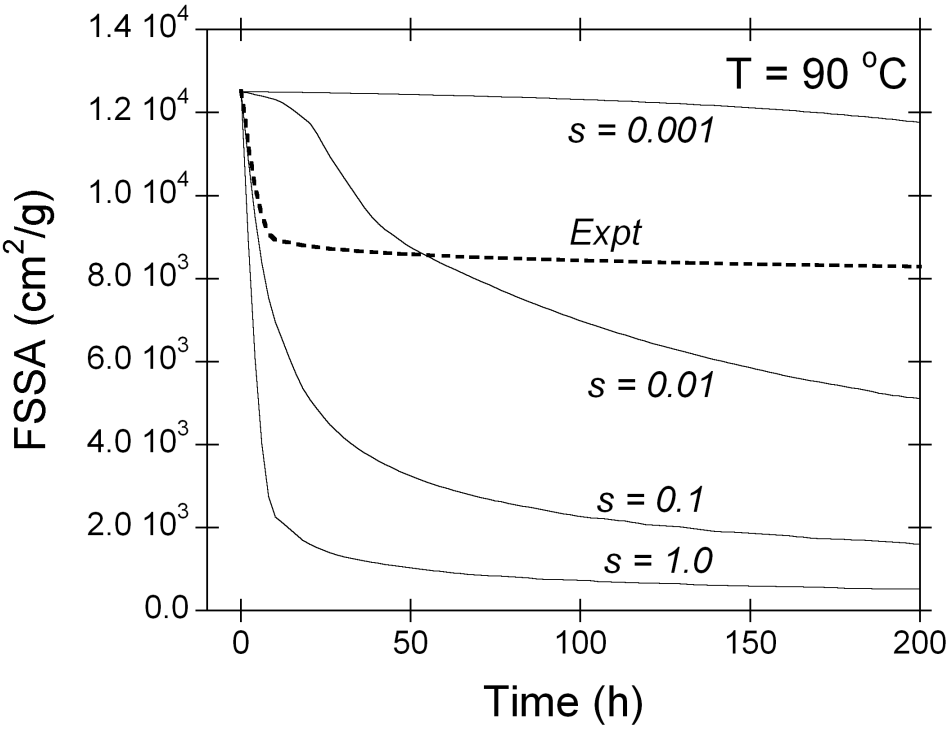

Fig. 6. (top) Model bimodal initial particle size distribution used with eqs. 6 through 9; (bottom) computed FSSA evolution at T = 90 °C for various constant (i.e. time-independent) values of the roughness parameter *s*. The experimental curve (from Fig. 1) is indicated by the dashed line.

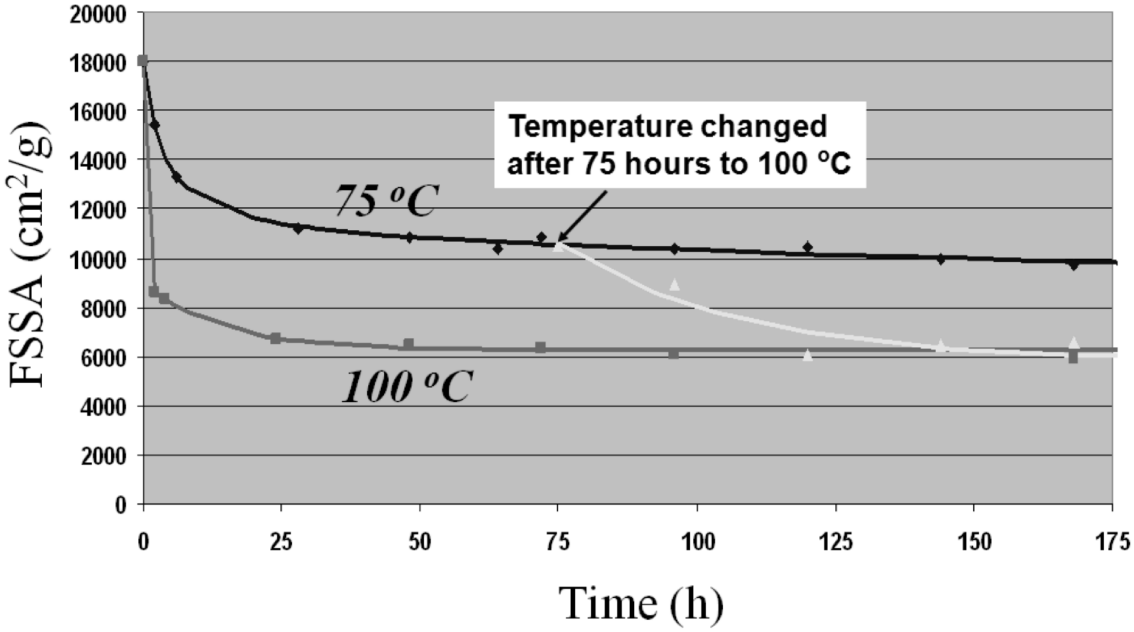

Fig. 7. Effect on FSSA evolution upon increasing the temperature from 75 °C to 100 °C in the middle of annealing. When the temperature is switched from 75 °C to 100 °C (at t = 75 hours) the sample displays a faster rate of FSSA loss until the FSSA evolution curve reaches that corresponding to 100°C. Note that this sample has an initial FSSA value of 1.8×10^3 cm^2/g, which is higher than that used in the experiment of Fig. 1. Experimental data is courtesy of ref. [7].